Study of Fatigue Crack Initiation Mechanism on an Armco Iron by Dissipation Assessments and Microstructural Observations

Chow Wang, Antoine Blanche, Danièle Wagner, André Chrysochoos, Claude Bathias

Study of Fatigue Crack Initiation Mechanism on an Armco Iron by Dissipation Assessments and Microstructural Observations

C. Wang[1], A. Blanche[2], D. Wagner[1], A. Chrysochoos[2], C. Bathias[1]

[1] University Paris Ouest Nanterre– LEME Laboratory – 50, rue de Sèvres – 92410 VILLE D'AVRAY – France, *Corresponding author : D. Wagner, daniele.wagner@u-paris10.fr*
[2] University Montpellier 2 – LMGC Laboratory, CNRS – Place Eugène Bataillon – 34095 MONTPELLIER – France

Abstract*. In the Low Cycle and High Cycle Fatigue regime, the first visible signs under an optical microscope of fatigue crack initiation are the occurrence of Persistent Slips Bands followed by the extrusion/intrusion formation on the specimen surface. In this study, the first signs of fatigue crack initiation were studied in the HCF domain on a body centred cubic Armco iron (with 80ppm of carbon content).The tests were performed on a piezoelectric fatigue machine on plate specimens. During the tests, the microstructure evolution was observed by optical microscope, and the temperature recording on the specimen surface was achieved by an infrared focal plane array camera. From the temperature recording, the intrinsic dissipation profile along the specimen gage part was calculated using a local expression of the heat diffusion equation. The results showed that above a stress level, Slips Marks can be clearly observed on the surface specimen, and related to the intrinsic dissipation distribution. Observations under a Scanning Electron Microscope on the specimen surface and the fracture surface are related to stage I and stage II of fatigue damage.*

INTRODUCTION

Whatever the fatigue domain, the fatigue crack mechanism consists of an initiation crack stage (stage I) and a propagation stage (stage II). For materials without inclusions with a single phase, the first damage events in the stage I are due to the occurrence of Slips Marks (SM) on the specimen surface [1,2]. In fcc materials (which are the most studied materials), these SM are called Persistent Slips Bands (PSB), with a particular dislocation structure beneath the PSB [3]. In bcc materials (Armco iron), the identification of these SM with PSB is matter for debate [3-8]. The reason lies in the very different temperature and strain rate dependent dislocation glide behaviour in bcc metals, as compared to fcc metals. Moderate increase of temperature, low cyclic strain rates and alloying by substitutional atoms (e.g. in Fe-Si) and interstitial atoms (e.g. C and N in α-iron) make the dislocation glide modes of bcc metals more similar to those of fcc metals and then, "PSBs" may be observed.

The beginning of the crack propagation stage with striations occurrence (stage II) has been studied previously by the temperature recording on the specimen surface during the test [9-10], which allows the determination of the number of cycles at crack initiation. In this paper, from the temperature recording on the specimen surface of an Armco iron during fatigue tests, the intrinsic dissipation profile along the specimen gage part was calculated using a local expression of the heat diffusion equation. Besides, fractographic observations were performed on the specimen surface and fracture surface.

MATERIAL

The studied material is a polycrystalline α iron whose chemical composition is given in Table1.The carbon content is 80ppm. The microstructure is ferrite with equiaxe grains. The inclusion size is less 1.5μm. The ferrite grain size is included in 10 to 40 μm. No specifically orientation was observed by EBSD. Yield Stress is 240 MPa and Ultimate Tensile Stress is 300MPa.

Table 1: Chemical composition of studied material

C	P	Si	Mn	S	Cr	Ni	Mo	Cu	Sn	Fe
0.008	0.007	0.005	0.048	0.003	0.015	0.014	0.009	0.001	0.002	Balance

EXPERIMENTAL PROCEDURE

Mechanical and Thermal Procedure

Tests were performed on a piezoelectric fatigue machine designed by C. Bathias and co-workers [11].

An infrared camera was used to record the temperature evolution during the test.

For the reason of surface observation condition by IR camera, a new design of 1 mm flat specimen (Fig. 1) was used to carry out fatigue tests. Specimen, special attachment and piezoelectric fatigue machine constituted the resonance system working at 20kHz. The cyclic loading is tension-compression (R = -1).

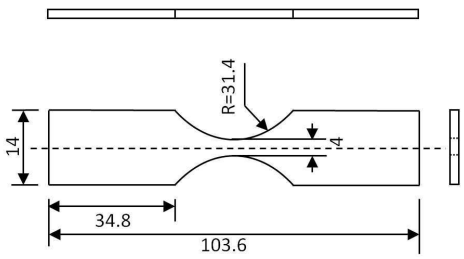

Figure 1: Design of flat specimen (unit: mm)

Before testing, both sides surface of the flat specimen were polished until the roughness less than R0.2. One side surface of the flat specimen was etched and another side painted in black color to have the surface emissivity close to 1.
From the temperature measurements, the intrinsic dissipation was determined using a 2D thermal model (see corresponding section).

Tests
Fatigue tests were periodically interrupted, and the stress level was increased until the specimen fracture was obtained. For the sample reported here, the test was conducted as described in Table 2.

Table 2: Fatigue tests

Test	Number of cycles	Stress σ_a (MPa)
Test 1	10^7	80
Test 2	10^7	90
Test 3	10^7	100
Test 4	10^7	110
Test 5	5.10^6	120

During the last run (test 5) with a stress of 120MPa, the specimen was broken.

DETERMINATION OF INTRINSIC DISSIPATION

From temperature fields to heat source distributions, a heat diffusion model has been developed to estimate the intrinsic dissipation from temperature measurement fields during fatigue tests. The local, compact expression of the heat diffusion equation can be written as:

$$\rho c\dot{T} - k\Delta T = s \qquad (1)$$

Where $T(x,y,z,t)$ is the temperature, ρ the mass density, C the heat capacity, k the thermal conduction coefficient and s(x,y,z,t) stands for the volume heat source. It can be shown assuming some hypothesis [12] that the 2D heat diffusion model can be rewritten as:

$$\rho C\left(\frac{\partial \theta}{\partial t} + \frac{\theta}{\tau}\right) - k\left(\frac{\partial^2 \theta}{\partial x^2} + \frac{\partial^2 \theta}{\partial y^2}\right) = s = s_{the} + d_1 \qquad (2)$$

with $\theta(x,y,t) = T - T_0$ the temperature variation, T_0 the room temperature, d_1 the intrinsic dissipation and s_{the} the thermoelastic source. The time constant τ characterizes the perpendicular heat exchanges between front and back specimen faces and the surroundings.

Taking the loading frequency (20 kHz) and the maximum frame rate of the IR camera (100 Hz) into account, the periodic thermoelastic sources are in this situation out of reach. It is also assumed that the widthwise heat losses are negligible compared with the lengthwise ones so that:

$$\rho C\left(\frac{\partial \theta}{\partial t}+\frac{\theta}{\tau}\right)-k\left(\frac{\partial^2 \theta}{\partial x^2}\right)=d_1 \qquad (3)$$

The last stage is to compute d_1 estimating the different partial derivative operators, using discrete, noisy thermosignals. Local spatiotemporal fitting was used to approximate the temperature field by this function:

$$\theta^{app}=P_1(x,y)t+P_2(x,y) \qquad (4)$$

Where $P_i(x,y)$ are second-order polynomials in x and y. These polynomials are finally identified using a least-squares method and then used to compute the intrinsic dissipation.

RESULTS AND DISCUSSION

Thermal results

Fig. 2 shows the temperature recordings (for the different applied stresses) versus the number of cycles. As previously published [9], the temperature has a sharp increase at the beginning of the test and tends progressively towards an asymptotic if there is no crack. Higher is the stress, higher is the temperature level.

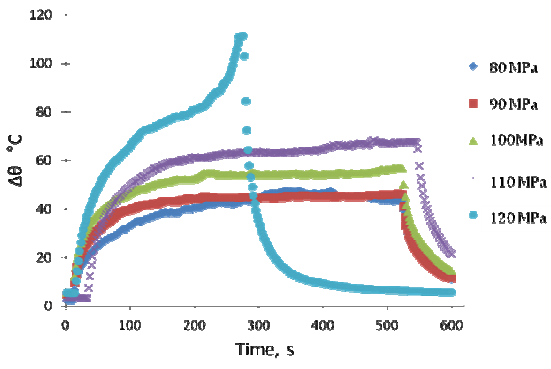

Figure. 2 Temperature evolution versus the number of cycles for different stress levels

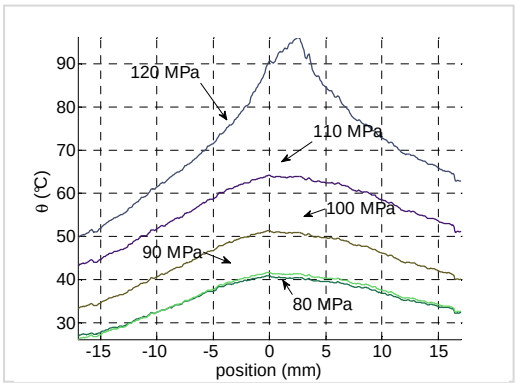

Figure. 3 temperature evolution along the length of specimen

If no crack, the highest temperature is always found close to the centre section of specimens where corresponds the highest stress distribution. Fig 3 shows the temperature evolution along the specimen length (for the different applied stresses)

Due to the horn (which increases the conduction phenomenon), the temperature profile is not symmetric. The top of the specimen (near the horn) is colder than the specimen bottom. When the specimen is tested at higher stress, the crack takes place. Fig. 4 shows infrared thermal images associated with different points of the time course of the mean temperature averaged over a small centred zone for the highest stress leading to fatigue fracture.

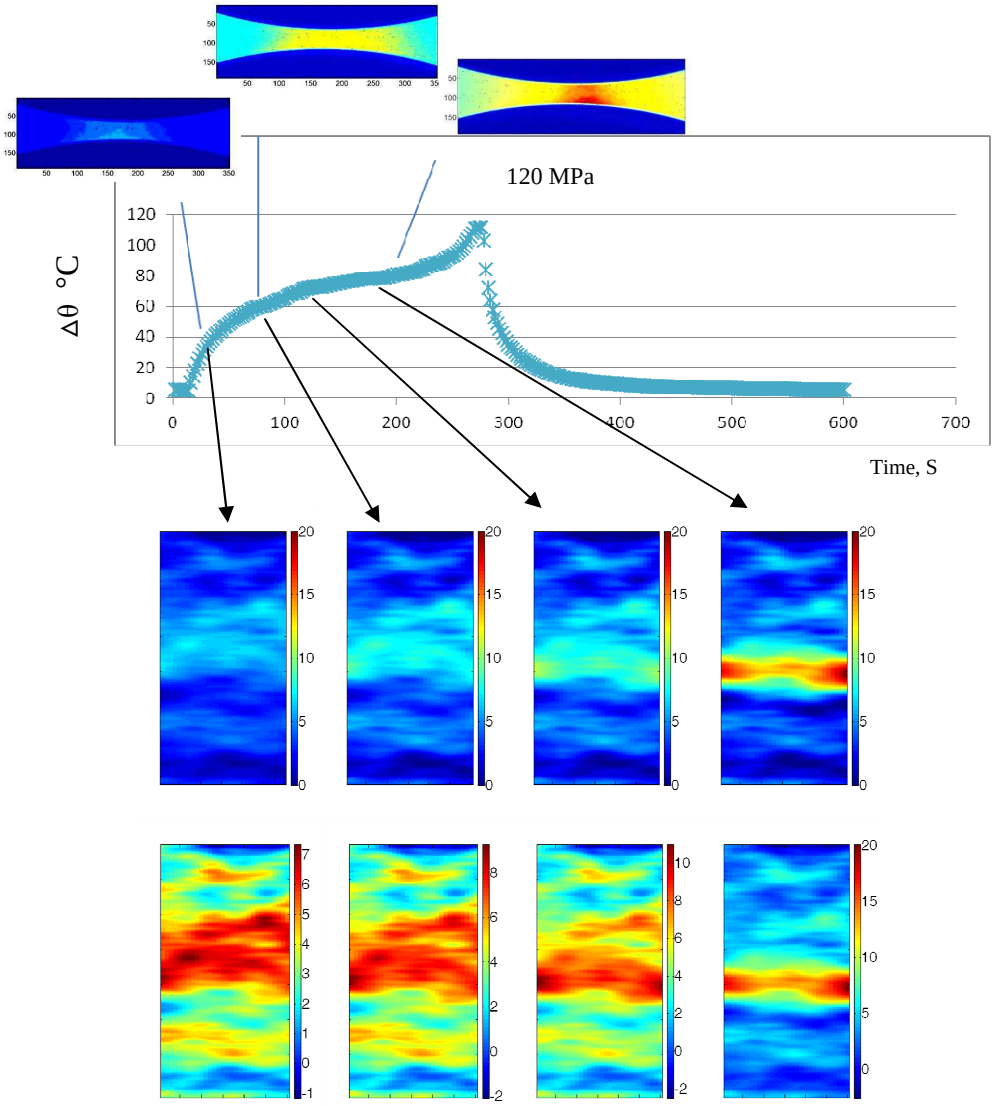

Figure. 4 Thermal thermo-graph and intrinsic dissipation fields for different number of cycles

The intrinsic dissipation fields on the specimen surface are shown in Fig 4. The abscissa corresponds to the specimen width and the ordinate to the length. At the beginning of the test, the intrinsic dissipation is very low (~ 5°C/s) to reach 20°C/s few seconds before the fracture. For the pictures 4, the intrinsic dissipation appears higher close to the centre section of the specimen in relatively good agreement with the stress concentration along the specimen. In this section, the dissipation is lower in a portion located around the middle of the specimen, always in agreement with the stress concentration profile in this centre section. In pictures 4, in centre section, the intrinsic dissipation is the highest on the right side, which corresponds to the initiation of the fracture (see fractographic observations). Note that the intrinsic dissipation is the trace of the specific heat sources in the material subjected to fatigue loading.

Fractographic Observations

As previously reported in the megacycle domain for Armco iron, the first occurrence damage is Slips Marks which are identified as Persistent Slips Bands (PSB) [7]. After removing a thin layer, it appears just below the PSB, transgranular microcracks (intrusion/extrusion). Sometimes, the first damage equally occurs in grain boundary. The fracture surface was observed by Scanning Electron Microscope. On the fatigue fracture surface, it can be distinguished three areas (Fig.5a): stage I, stage I→II, stage II. The stage I corresponds to the initiation stage and is correlated with the transgranular intrusion/extrusion (Fig.5b) or intergranular microcracks. When the intrusion/extrusion is transgranular, the grain traces are visible on the fracture surface with “steps” oriented in different directions, steps which are due to PSB and intrusion/extrusion formation. When the microcrack is intergranular, the grain traces are also visible, but the grain surface appears more flat. The stage I→II (Fig.5c) is the beginning of the propagation. In this stage, some striations are visible perpendicular to the direction of crack propagation besides the steps of stage I.

The stage II (Fig.5d) is the crack propagation stage with visible striations perpendicular to the crack propagation direction.

The observation of the polished surface where the temperature variation was recorded shows PSB occurrence over a distance of about 3 mm (one side) and 3.3 mm (other side) from the fracture surface. The Fig.6 is a picture just below the fracture surface where the PSB are present in many grains.

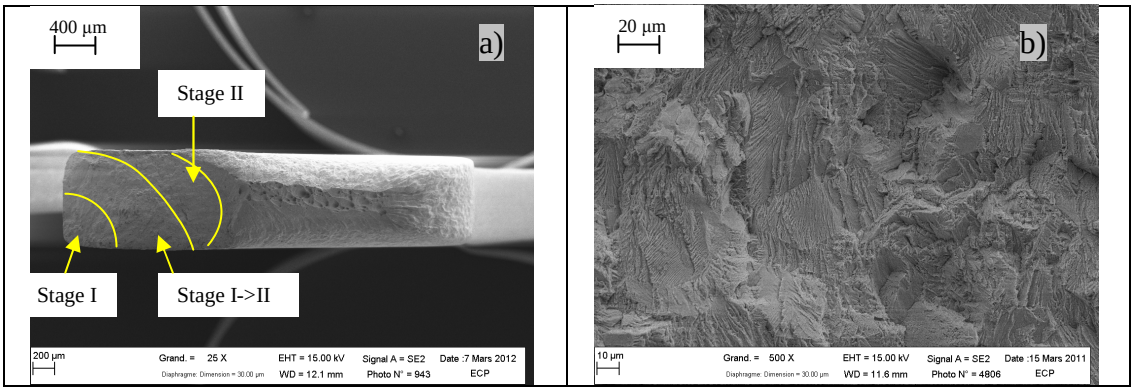

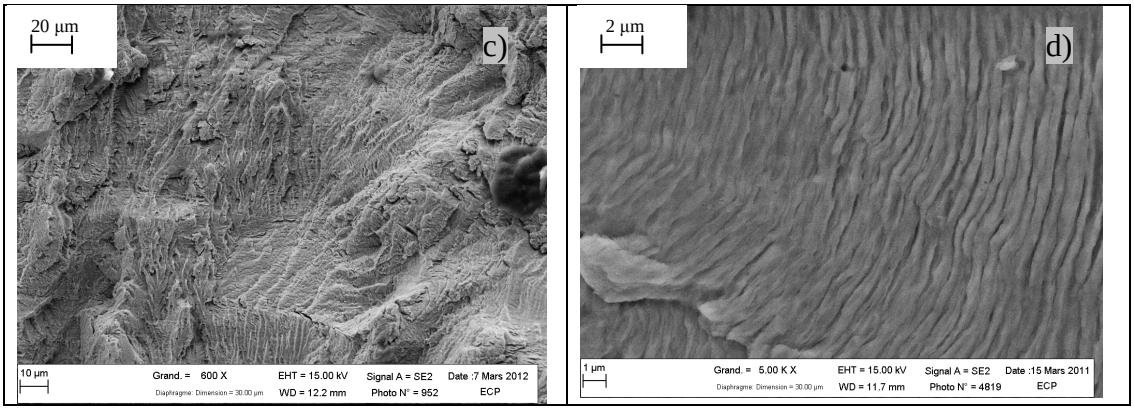

Figure.5 Fractographic observation of the fracture surface.(a)Fracture surface (b) crack initiation site (stage I) (c)transition stage (stage I-> II) (d) striation(stage II)

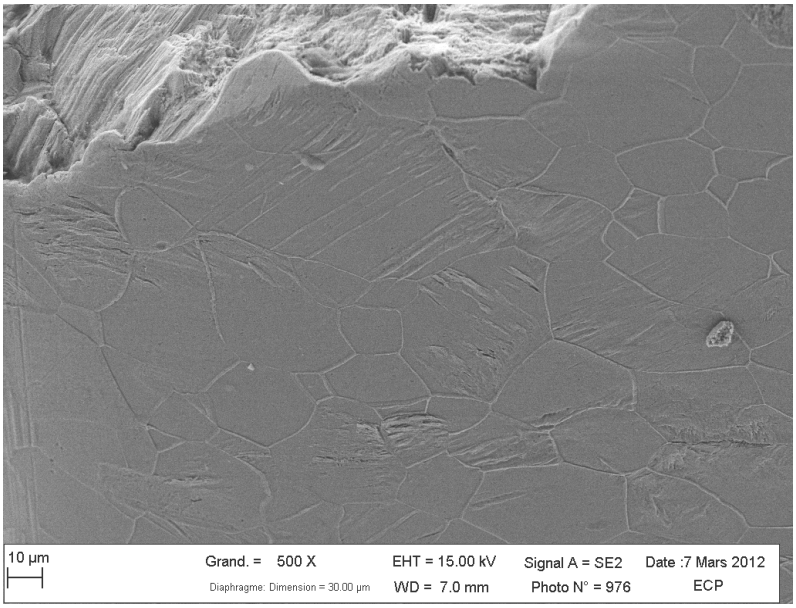

Fig 6 SEM observation of the polished surface just beneath the crack initiation site

Discussion

The polished surface observed by SEM (Fig.6) is the polished surface where the temperature was recorded and the initiation stage (stage I) corresponds to the highest dissipation d_1 on the right side seen in Fig.4. The distance measurement over which d_1 is higher than 10 °C/s on the specimen length corresponds to about 5.7mm, that is to say in very good agreement with the length on each side of fracture surface where PSB are occurred (6.3mm). So, the PSB are the specific heat sources at the origin of crack initiation (stage I).

If we calculated the effective fatigue stress intensity factor at the end of stage I, $\Delta K_{eff} = \Delta K_I/2 = 3.8$ MPa$\sqrt{m}$, it is approximately equal to E$\sqrt{b}$ =3.4MPa$\sqrt{m}$ for Armco iron

(where E = 210GPa and b = 0.265nm). It is excellent agreement with the Herzberg's [13] work about propagation threshold of fatigue crack propagation rate (measured at conventional frequency fatigue test).

CONCLUSION

In this study, the first signs of fatigue crack initiation were studied in the HCF domain on a body centred cubic Armco iron (with 80 ppm of carbon content).The tests were performed on a piezoelectric fatigue machine on plate specimens. During the tests, the temperature recording on the specimen surface allows the intrinsic dissipation field determination. The main conclusions are:

- The localization of the intrinsic dissipation occurs in the specimen section where the fracture takes place.
- In this section, the dissipation d_1 is maximum on the specimen right side where the fatigue crack initiation takes place.
- The height on the specimen length where d_1 is high corresponds to the height where PSB are present. So, the irreversible PSB development induces is the main energy dissipation sources.

ACKNOWLEDGEMENT

This research was supported by the grant from the project of Microplasticity and energy dissipation in very high cycle Fatigue (DISFAT, project No. ANR-09-BLAN-0025-09), which funded by the National Agency of Research, France (ANR).

REFERENCES

1. Suresh, S. (2006) In : *Fatigue of Materials*, pp 37- 162
2. Bathias,C.,Pineau, A. (2008) In : *Fatigue des matériaux et des Structures 1*, pp85-246
3. Mughrabi, H. (1980). In : *The Strength of Metals and Alloys*, pp.1615-1639, Haasen,P., Gerold, V.,Kostorz, G., (Ed.), Pergamon Press, Oxford
4. Mughrabi, H., Herz, K., Stark, X. (1976) *Int Journal of Fracture* **17**,193-320
5. Mughrabi, H., Wüthrich, Ch. (1976) *Philosophical Magazine* **A33**, 963-984
6. Mughrabi, H., Ackermann, F., Herz, K. (1979) In: ASTM STP 675, pp 69-105
7. Klesnil, M., Lukas, P. (1965) *J. of the Iron and Steel Institute* **203**, 1043 – 1048
8. Sommer, C., Mughrabi, H., Lockner, D. (1998) *Acta Mater*. **46**, 1527-1536
9. Wagner, D., Ranc, N., Bathias**, C.,** Paris, P. (2009) *Fat. Fract. Engng Mater Struct* **33**, 12-21
10. Ranc, N., Wagner**,** D**.,** Paris, P.C. (2008) *Acta Materiala* **56,** 4012-4021
11. Bathias, C., Paris, P. C. (2004). In : *Gigacycle Fatigue in Mechanical Practice*, pp 51-76, Marcel Dekker, New York
12 Berthel, B., Wattrisse, B., Chrysochoos, A. & Galtier, A. (2007). Blackwell Publishing Ltd, **43**, 273-279
13 P.C Paris, H. Tada, J. Keith Donald (1999). *International Journal of Fatigue*, **21**, 35-46